Journal of Membrane Science 603 (2020) 117995

Contents lists available at ScienceDirect

Journal of Membrane Science

journal homepage: http://www.elsevier.com/locate/memsci

Solid polymer electrolyte supported by porous polymer membrane for all-solid-state lithium batteries

Yerin Seo, Yun-Chae Jung, Myung-Soo Park, Dong-Won Kim *

Department of Chemical Engineering, Hanyang University, Seongdong-gu, Seoul, 04763, Republic of Korea

ARTICLE INFO

Keywords:
Poly(ε-caprolactone)
Polymer membrane
Solid polymer electrolyte
All-solid-state battery
Poly(ether imide)

ABSTRACT

Solid polymer electrolytes composed of poly(ε-caprolactone) (PCL) and lithium bis(trifluoromethane) sulfonylimide (LiTFSI) salt were prepared for investigating their electrochemical properties. The optimized solid polymer electrolyte showed ionic conductivities of 2.5×10^{-5} and 1.6×10^{-4} S cm^{-1} at room temperature and 55 °C, respectively. Dimensional stability was improved by infiltrating PCL-based solid polymer electrolyte into the porous polymer membranes prepared from poly(ether imide) (PEI), polyacrylonitrile (PAN) and non-woven polypropylene (PP) membranes. Due to the highly porous nature and good compatibility of the PEI membrane toward the PCL-based solid polymer electrolyte, a solid-state Li/$LiNi_{0.6}Co_{0.2}Mn_{0.2}O_2$ cell assembled with a solid polymer electrolyte employing a PEI membrane exhibited the best cycling performance. Based on our results, this highly porous PEI membrane is proposed as a promising supporting membrane for enhancing the mechanical stability of amorphous solid polymer electrolytes for applications in all-solid-state lithium batteries.

1. Introduction

Rechargeable lithium-ion batteries (LIBs) have become the main power sources for portable electronic devices, and their applications have rapidly expanded to electric vehicles and large-scale energy storage systems based on their excellent cycling performance with respect to energy density and cycle life [1–5]. Although current commercialized LIBs employing liquid electrolytes exhibit superior cycle performance compared to other rechargeable battery systems, there are still concerns related to the use of liquid electrolytes, such as solvent leakage, high volatility and flammability, which make full utilization for large capacity applications very challenging due to the safety issues [5,6]. As a strategy for enhancing battery safety, all-solid-state lithium battery assembled with a solid-state electrolyte has gained great attention [7–12]. Among the various types of solid electrolytes, solvent-free polymer electrolytes have attractive properties such as absence of leakage problem, non-flammability, easy processing for producing a thin film, low cost, design flexibility, cuttable shapes and good interfacial contacts with electrodes. Although there are some limits in all-solid-state lithium metal batteries using solid polymer electrolyte such as low energy density and cycling stability related with Li metal, they are promising for various niche applications such as wearable devices, flexible displays, highly safe electric vehicles, tailorable and penetrable batteries [13–15]. To date, poly(ethylene oxide)(PEO)-based solid polymer electrolytes have been intensively studied for LIB applications, since PEO has strong solvating properties for dissolving lithium salts and high chain flexibility with a low glass transition temperature (T_g: ~ −60 °C) [16–19]. However, they have significant drawbacks such as low ionic conductivity (<10^{-6} S cm^{-1}) at ambient temperature due to the semi-crystalline nature of PEO and low oxidative stability at higher voltage than 4.0 V. As an alternative to PEO-based polymers, many non-PEO polymers with high solvation ability and low glass transition temperature have been actively studied to produce solid polymer electrolyte with high ionic conductivity [20–29]. Among the investigated polymer hosts for preparing solid polymer electrolytes, polyester-based polymers such as poly(ethylene adipate), poly(butylene adipate), poly(ethylene succinate) and poly(ε-caprolactone) (PCL) have been studied, because they can effectively dissolve lithium salts, thus providing a sufficient number of free ions and exhibit higher anodic stability than PEO-based solid polymer electrolytes [30–37]. Some of polyester-based solid polymer electrolytes exhibited high ionic conductivities at ambient and high temperatures, however, their mechanical properties were often poor and thin free-standing films could not be obtained without a thermal curing process.

In our work, we prepared solid polymer electrolytes with semi-crystalline PCL and lithium bis(trifluoromethane) sulfonylimide

* Corresponding author.
E-mail address: dongwonkim@hanyang.ac.kr (D.-W. Kim).

https://doi.org/10.1016/j.memsci.2020.117995
Received 1 August 2019; Received in revised form 19 February 2020; Accepted 22 February 2020
Available online 4 March 2020

(LiTFSI), which exhibited fully amorphous nature and high ionic conductivity at high salt concentration. To improve their dimensional stability without thermal cross-linking process, the PCL-based solid polymer electrolyte was penetrated into highly porous polymer membranes that had been prepared from poly(ether imide) (PEI), polyacrylonitrile (PAN) and polypropylene (PP). The membrane-supported solid polymer electrolyte was then applied to all-solid-state lithium cell composed of a lithium anode and a $LiNi_{0.6}Co_{0.2}Mn_{0.2}O_2$ cathode. Cycling performance of the Li/$LiNi_{0.6}Co_{0.2}Mn_{0.2}O_2$ cells using different porous polymer membrane was evaluated and the best type of polymer membrane was suggested as a supporting membrane for all-solid-state lithium cell.

2. Experimental

2.1. Materials

PCL (Mn = 80,000) and PAN (Mw = 150,000) were purchased from Sigma-Aldrich and used after a vacuum drying at 40 °C for 24 h. Non-woven PP membranes (thickness: 100 μm, porosity: 70%) and LiTFSI (battery grade) were purchased from Nippon Kodoshi Corporation and Panax Etec Co. Ltd., respectively, then were used after drying in a vacuum oven at 100 °C for 24 h. Pyromellitic dianhydride (PMDA, Sigma-Aldrich), 4,4′-oxydianiline (ODA, Sigma-Aldrich) were used after vacuum drying at 60 °C for 12 h. Tetrahydrofuran (THF, anhydrous, Alfa Aesar), N,N-dimethylformamide (DMF, anhydrous, Sigma-Aldrich), 1-methyl-2-pyrrolidone (NMP, anhydrous, Sigma-Aldrich) and N,N-dimethylacetamide (DMAc, anhydrous, Sigma-Aldrich) were used as received.

2.2. Synthesis of poly(amic acid)(PAA)

Poly(amic acid) (PAA) was synthesized via polycondensation reaction of dianhydride (PMDA) and diamine (ODA). ODA (13.8 g, 68.8 mmol) was added into a four-neck round-bottomed flask containing anhydrous NMP solvent (100 g) under a nitrogen atmosphere. The resulting solution was cooled and maintained at −10 °C using a bath circulator. PMDA (15.0 g, 68.8 mmol) dissolved in NMP (43.2 g) was added to the flask to react with ODA. The solution was stirred for 24 h, and it finally became a viscous yellowish PAA solution. The PAA solution was precipitated in a mixed solvent of water and methanol (3:1 by volume) and filtered to remove the residual solvent. The obtained PAA was dried in a vacuum oven at 80 °C for 12 h.

2.3. Preparation of electrospun PEI and PAN membranes

Porous PEI and PAN membrane were prepared using the electrospinning method. PAA was first dissolved in DMAc at a concentration of 33.0 wt% and the solution was fed through a capillary line using a plastic syringe. A high voltage of 18 kV was applied to the needle and the flow rate of the spinning solution was fixed at 0.4 ml h^{-1} using a syringe pump. The tip-to-collector distance was 15 cm and the metal drum was rotated at 100 rpm. The electrospun PAA membrane was collected on an aluminum foil-wrapped drum and dried overnight in a vacuum oven at 80 °C. To induce the imidization of PAA, the obtained membrane was baked in an electric furnace. The temperature was increased at a rate of 5 °C min^{-1} up to 300 °C and maintained for 2 h under a nitrogen atmosphere. Finally, the porous PEI membrane with a thickness of 60 μm was obtained. The electrospun PAN membrane was also obtained in a similar way, except for necessary variance in the electrospinning conditions. In the case of the PAN membrane, 12 wt% PAN solution in anhydrous DMF was used, and the applied voltage and the flow rate were adjusted to 15 kV and 0.6 ml h^{-1}, respectively. The thickness of electrospun PAN membrane was controlled to 60 μm.

2.4. Preparation of the solid polymer electrolytes

PCL and LiTFSI with different molar ratios were dissolved in an anhydrous THF at 60 °C for 12 h, as given in Table 1. Herein, the salt concentration in the solid polymer electrolyte is expressed as a molar ratio of repeat unit (RU) of PCL to LiTFSI salt.

A doctor blade was used to cast the solution onto a Teflon plate and the THF solvent was allowed to slowly evaporate at room temperature in a glove box. The obtained solid polymer electrolyte was further dried in a vacuum oven at 80 °C for 12 h to completely remove any residual solvent. To prepare the membrane-supported solid polymer electrolytes, the porous polymer membranes (PEI, PAN, PP) were immersed in the polymer electrolyte solution (PCL and LiTFSI dissolved in THF) for 24 h, as depicted in Fig. 1. The resulting membranes were removed, allowing slow evaporation of the solvent at room temperature. After evaporation of THF, the membrane-supported solid polymer electrolytes were further dried in a vacuum oven at 80 °C for 24 h. After vacuum drying, the free-standing flexible thin film was obtained. All the procedures for preparing the solid polymer electrolytes were performed in a glove box filled with argon gas.

2.5. Electrode preparation and cell assembly

The lithium anode was prepared by pressing a lithium foil (200 μm, Honjo Metal Co., Ltd.) onto a copper current collector. The composite $LiNi_{0.6}Co_{0.2}Mn_{0.2}O_2$ cathode was prepared by casting a THF-based viscous slurry containing $LiNi_{0.6}Co_{0.2}Mn_{0.2}O_2$, PCL, LiTFSI, and Super P carbon with a weight ratio of 60.0 : 18.3: 11.7 : 10.0 onto Al foil. PCL was used as a binder as well as Li^+-ion conductor in the composite cathode. The electrode was roll-pressed to enhance the particulate interfacial contact and adhesion to the Al current collector. The electrode was then dried under vacuum for overnight at 80 °C. The active mass loading in the composite cathode was about 3.5 mg cm^{-2}. A solid-state Li/$LiNi_{0.6}Co_{0.2}Mn_{0.2}O_2$ cell was assembled by sandwiching the membrane-supported solid polymer electrolyte between the lithium anode and the $LiNi_{0.6}Co_{0.2}Mn_{0.2}O_2$ cathode in a coin-type-cell (CR 2032). The cell was aged at 55 °C for 24 h to promote the interfacial contact between solid polymer electrolyte and electrodes. All of the cells were assembled in the glove box filled with argon gas.

2.6. Characterization and measurements

Differential scanning calorimetry (DSC) measurements were performed using a TA instrument (SDT Q600/DSC Q20) at a heating rate of 5 °C min^{-1} in the temperature range of −80 to 100 °C under a dry nitrogen atmosphere. The porosity of electrospun membranes was determined by immersing samples into n-butanol for 1 h and calculated according to Equation (1):

$$\text{Porosity}(\%) = \frac{m_b/\rho_b}{m_b/\rho_b + m_s/\rho_s} \times 100, \quad (1)$$

where m_b is the weight of absorbed n-butanol, m_s is the weight of the membrane, ρ_b is the density of n-butanol and ρ_s is the density of the membrane [38,39]. Attenuated total reflection Fourier-transform infrared (ATR-FTIR) spectra of the solid polymer electrolytes were

Table 1
Composition of PCL-based solid polymer electrolytes.

Solid polymer electrolyte	PCL (wt.%)	LiTFSI (wt.%)	[RU]/[LiTFSI]
PCL-2	44	56	2/1
PCL-4	61	39	4/1
PCL-6	70	30	6/1
PCL-8	76	24	8/1
PCL-16	86	14	16/1

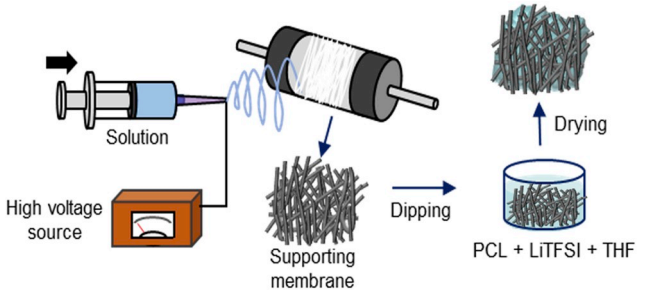

Fig. 1. Schematic illustration for preparing the membrane-supported solid polymer electrolytes.

obtained using a Nicolet iS50 Fourier-transform infrared spectrometer (Thermo Scientific) in the wavenumber range of 400–4,000 cm^{-1}. The morphologies of the porous membranes and membrane-supported solid polymer electrolytes were examined using field-emission scanning electron microscopy (FE-SEM, JEOL JSM-6330F). For ionic-conductivity measurements, the solid polymer electrolyte was sandwiched between two disk-like stainless-steel electrodes. AC impedance measurements were performed using a Zahner Elektrik IM6 impedance analyzer in the frequency range of 10 Hz to 1 MHz with an amplitude of 10 mV at different temperatures. Each sample was allowed to equilibrate for 1 h at the required temperature before measurement. Linear sweep voltammetry (LSV) was performed to investigate the electrochemical stability of the solid polymer electrolyte on a platinum working electrode, with lithium metal as the counter and reference electrodes, at a scanning rate of 1.0 mV s^{-1} and 55 °C. Charge and discharge cycling test of the solid-state Li/$LiNi_{0.6}Co_{0.2}Mn_{0.2}O_2$ cells was conducted at a constant current rate in the voltage range of 3.0–4.2 V using battery test equipment (WBCS 3000, Wonatech) at 55 °C.

3. Results and discussion

Fig. 2a shows the DSC thermograms of PCL and PCL-based solid polymer electrolytes with different salt concentrations. The melting transition of PCL was clearly observed around 55.9 °C and its crystallinity was calculated as 40.3% based on its heat of melting. As shown in the figure, the degree of crystallinity gradually decreased with increasing salt concentration, and the melting peak completely disappeared at high salt concentration, indicating the solid polymer electrolyte becomes fully amorphous above [RU]/[LiTFSI] = 4.0. The reduction of crystallinity is caused by intermolecular physical cross-linking through ion-polymer interactions occurred in the solid polymer electrolyte [40]. The T_g value of solid polymer electrolytes decreased with salt concentration. This result can be explained by the increased conformational mobility of the polymer backbone with increasing salt concentrations, as previously reported [22,28]. In addition, the plasticizing of polymer by LiTFSI is also attributed to the decrease in T_g of solid polymer electrolyte. Fig. 2b shows the temperature dependence of ionic conductivity for solid polymer electrolytes with different salt concentration. Semi-crystalline solid polymer electrolytes (PCL-16, PCL-8, PCL-6) showed an abrupt decrease in ionic conductivity around its melting temperature (T_m), which arises from its crystalline nature below T_m. On the other hand, the temperature dependence of ionic conductivity for fully amorphous solid polymer electrolytes (PCL-4, PCL-2) exhibited Vogel-Tamman-Fulcher (VTF) behavior over the temperature ranges investigated, indicating that ionic conduction in the amorphous solid polymer electrolyte mainly depends on the segmental motion of the polymer chain [41].

When comparing the ionic conductivity of the solid polymer electrolytes at the same temperature, the ionic conductivity was increased with salt concentration. As discussed earlier, the addition of LiTFSI into PCL polymer decreases the T_g of the solid polymer electrolyte, resulting

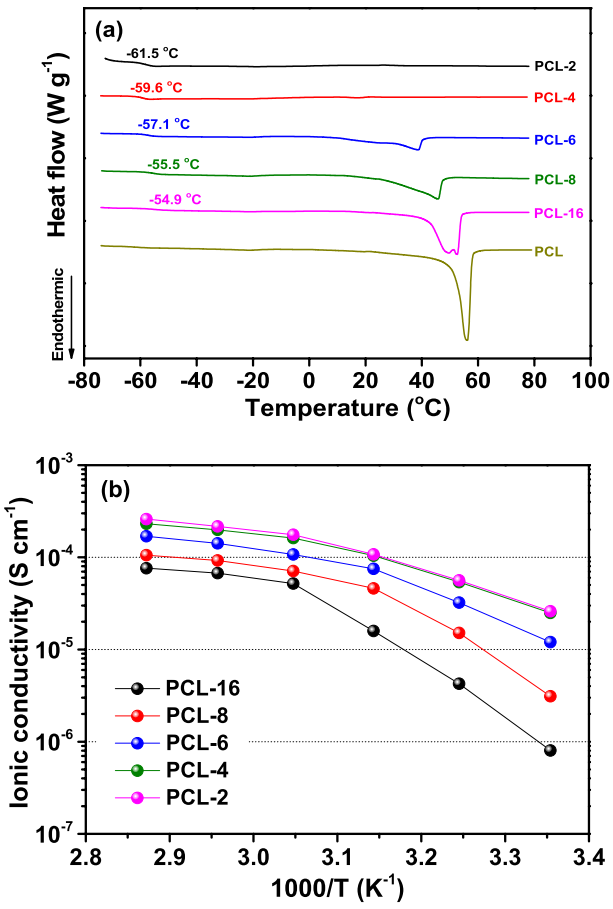

Fig. 2. (a) DSC thermograms of PCL and solid polymer electrolytes with different salt concentration and (b) temperature dependence of ionic conductivities of solid polymer electrolytes with different salt concentrations.

in improved ionic mobility. The number of free ions is also increased with LiTFSI concentration. Accordingly, the increase in ionic conductivity with salt concentration can be attributed to the increases in both ionic mobility and number of charge carriers. PCL-4 exhibited ionic conductivities of 2.5 × 10^{-5} and 1.6 × 10^{-4} S cm^{-1} at 25 and 55 °C, respectively. Ionic conductivity could be increased by further increasing the salt concentration over [RU]/[LiTFSI] = 2.0, however, the mechanical stability of solid polymer electrolyte became very weak and sticky.

The chain conformation of PCL and ion-polymer interactions in the solid polymer electrolyte were investigated by FT-IR analysis. FT-IR spectra of PCL and solid polymer electrolytes with different salt concentrations are presented in Fig. 3. The bands observed at 2865 and 2945 cm^{-1} in the spectrum of the PCL polymer (Fig. 3a) can be assigned to symmetric and antisymmetric stretching vibrations of CH_2 in the backbone of PCL, respectively [42]. As a LiTFSI salt was added into PCL, new bands appeared at 2915 and 2848 cm^{-1}, which corresponded to the CH_2 stretching vibrations of normal alkanes. This result indicates that the local segmental motion of PCL is enhanced with the addition of LiTFSI, which is well consistent with DSC results that the T_g values of solid polymer electrolyte decreased with increasing salt concentration. The band observed around 1730 cm^{-1} in the spectrum of PCL polymer (Fig. 3b) can be assigned to the stretching vibration of the free carbonyl group (C=O) in the main chain of PCL. A new peak arising from the ion-polymer interaction between carbonyl groups and Li^+ ions appeared around 1700 cm^{-1} when the LiTFSI salt was added.

The relative intensities of peaks at 1730 and 1700 cm^{-1} could be calculated, and the results are summarized in Table 2. From the table, it can be seen that the relative fraction of interacted C=O groups (1700

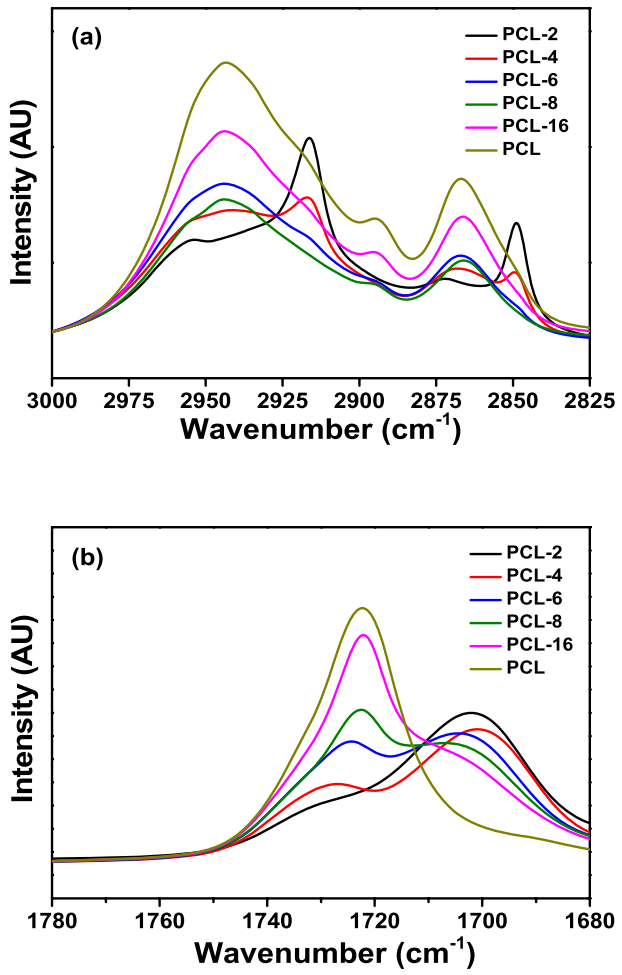

Fig. 3. FT-IR spectra of PCL and solid polymer electrolytes with different salt concentrations. (a) CH_2 stretching vibrational and (b) C=O stretching vibrational regions.

Table 2
Relative fraction of free and interacted carbonyl groups in the solid polymer electrolytes.

Solid polymer electrolyte	Free C=O (1730 cm^{-1})	Interacted C=O (1700 cm^{-1})
PCL-16	0.78	0.22
PCL-8	0.68	0.32
PCL-6	0.51	0.49
PCL-4	0.34	0.66
PCL-2	0.23	0.77

cm^{-1}) in the solid polymer electrolyte steadily increased with salt concentration, indicating that the number of dissociated ions was increased with the addition of LiTFSI into PCL.

PCL-2 and PCL-4 exhibited high ionic conductivities due to fully amorphous nature and high chain flexibility (low T_g), as discussed earlier. However, they are both very sticky, thus a dimensionally stable free-standing film is difficult to prepare with them. To overcome their poor mechanical property, the porous polymer membranes were employed as the supporting membrane. Highly conductive solid polymer electrolyte, PCL-4, was penetrated into the pores of the porous membranes prepared with PEI, PAN and PP, respectively. Fig. 4a–c shows the SEM images of porous membranes used as the supporting membranes in this study. They are characterized by highly porous structure. The membrane porosities were measured to be 78, 75 and 70% for PEI, PAN and PP membranes, respectively. The surface SEM images of membrane-supported solid polymer electrolytes in Fig. 4d–f demonstrate that the pores of the membranes are fully covered with solid polymer electrolyte without any voids or empty space.

From the cross-sectional SEM images of the membranes filled with solid polymer electrolyte (Fig. 4g–i), it was found that the membrane-supported solid polymer electrolytes exhibited somewhat different morphologies. When PEI and PAN were employed as the supporting membranes, the compact and dense morphology was obtained. In the case of the PP membrane, the rough cross section was observed. Such a difference in the cross-sectional morphologies may be mainly caused by the difference in affinity of polymer membranes with solid polymer electrolyte filled in the pores. It should be noted that the PCL-based solid polymer electrolyte is much more compatible with PEI or PAN than hydrophobic PP.

Fig. 5a shows the temperature dependence of ionic conductivities for membrane-supported solid polymer electrolytes. When filling solid polymer electrolyte into the porous polymer membranes, the ionic conductivity was decreased compared to those of solid polymer electrolyte (PCL-4) itself. The decrease in ionic conductivity can be attributed to blocking for ion transport, since the supporting polymer membranes (PEI, PAN, PP) are insulators by nature. The use of highly porous PEI membrane with high compatibility for the PCL-based solid polymer electrolyte resulted in the highest ionic conductivity. The PEI membrane-supported solid polymer electrolyte with a thickness of 65 μm showed a high ionic conductivity of 1.1×10^{-4} S cm^{-1} at 55 °C, and its mechanical strength was almost the same as that of the pristine PEI membrane. The electrochemical stability of membrane-supported solid polymer electrolytes was evaluated using LSV measurements at 55 °C, and the obtained linear sweep voltammograms are shown in Fig. 5b. As shown in the figure, the oxidative current started to increase around 4.6 V vs Li/Li^+ in the solid polymer electrolyte without supporting membrane, which can be attributed to the oxidative decomposition of PCL.

All of the membrane-supported solid polymer electrolytes exhibited slightly improved anodic stability compared to solid polymer electrolyte without a supporting membrane. The type of supporting membrane hardly affected the electrochemical stability of the membrane-supported solid polymer electrolytes. Based on these results, the membrane-supported solid polymer electrolytes exhibit high ionic conductivity and good electrochemical stability, which makes them suitable as solid electrolytes for application in an all-solid-state $Li/LiNi_{0.6}Co_{0.2}Mn_{0.2}O_2$ cell.

A solid-state $Li/LiNi_{0.6}Co_{0.2}Mn_{0.2}O_2$ cell was assembled by sandwiching the membrane-supported solid polymer electrolyte between the Li anode and composite $LiNi_{0.6}Co_{0.2}Mn_{0.2}O_2$ cathode, as schematically presented in Fig. 6.

The sticky PCL-based solid polymer electrolyte in the porous membrane and the composite $LiNi_{0.6}Co_{0.2}Mn_{0.2}O_2$ cathode assisted in enhancing the interfacial contacts between the electrolyte and the electrodes.

Fig. 7a shows the charge and discharge curves of the solid-state $Li/LiNi_{0.6}Co_{0.2}Mn_{0.2}O_2$ cell assembled with PEI membrane-supported solid polymer electrolyte, which are obtained at 55 °C and 0.1C rate. The cell initially delivered a discharge capacity of 167.2 mA h g^{-1} based on $LiNi_{0.6}Co_{0.2}Mn_{0.2}O_2$ material in the composite cathode. After the 100th cycle, the discharge capacity was decreased to 136.5 mA h g^{-1}, which corresponded to 81.6% of its initial discharge capacity. The capacity fading of the cell may be mainly caused by the gradual deterioration of the interfacial contacts of active material, conducting carbon and solid polymer electrolyte in the composite cathode, because the binding property of PCL is inferior to poly(vinylidene fluoride) (PVdF) that commonly is being used as a binder in the cathode for the commercialized lithium-ion cell. Fig. 7b presents the discharge capacities and coulombic efficiencies of the solid-state $Li/LiNi_{0.6}Co_{0.2}Mn_{0.2}O_2$ cells with different membrane-supported solid polymer electrolytes at 55 °C, as a function of cycle number. The coulombic efficiency of the cell was increased after the initial few cycles and reached an almost constant

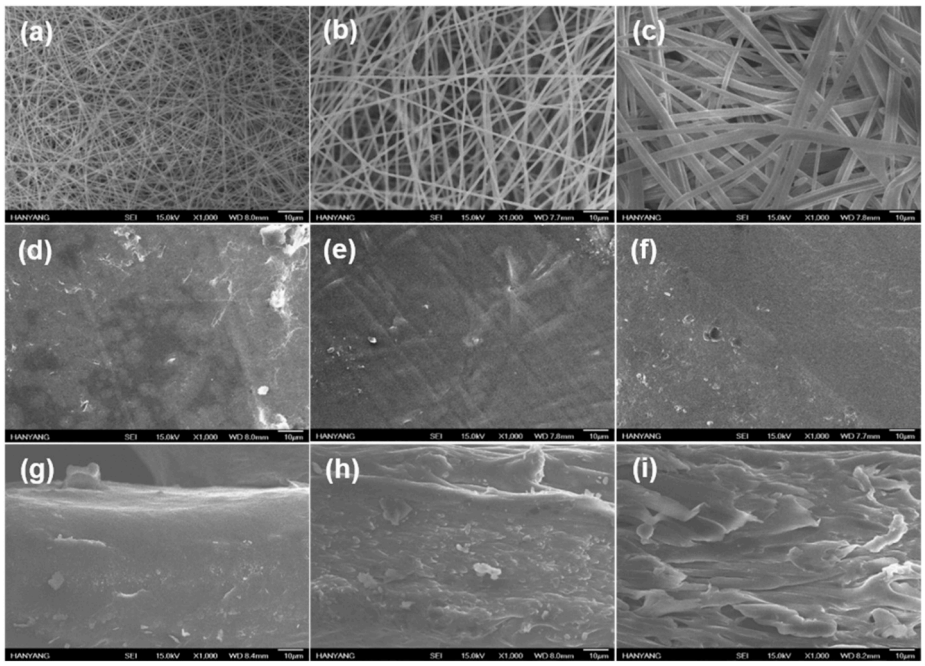

Fig. 4. SEM images of (a) PEI, (b) PAN and (c) PP membranes. Surface SEM images of membrane-supported solid polymer electrolytes prepared with (d) PEI, (e) PAN and (f) PP membranes. Cross-sectional SEM images of membrane-supported solid polymer electrolytes prepared with (g) PEI, (h) PAN and (i) PP membranes.

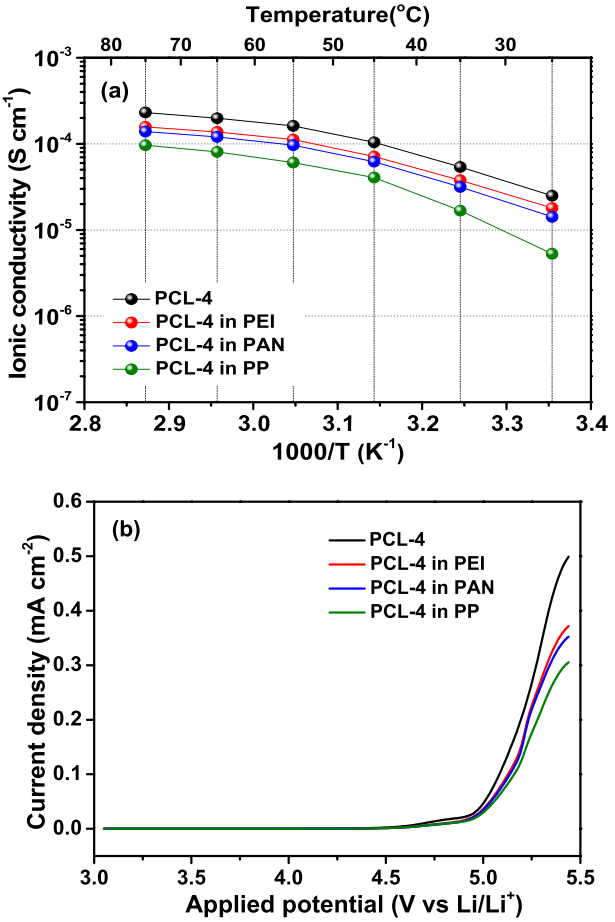

Fig. 5. (a) Temperature dependence of ionic conductivities of the membrane-supported solid polymer electrolytes and (b) linear sweep voltammograms of the membrane-supported solid polymer electrolytes at a scan rate of 1 mV s^{-1} and 55 °C.

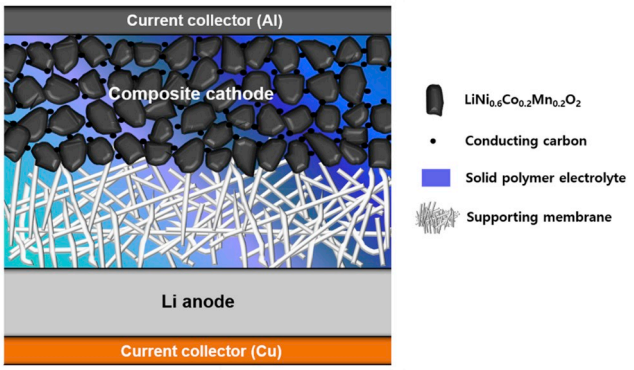

Fig. 6. Schematic presentation of solid-state Li/$LiNi_{0.6}Co_{0.2}Mn_{0.2}O_2$ cell assembled with membrane-supported solid polymer electrolyte.

value over 99.5% throughout repeated cycling. Among the cells investigated, the cell with PEI membrane-supported solid polymer electrolyte exhibited the best cycling performance in terms of discharge capacity and cycling stability. This result can be ascribed to the high porosity of the PEI membrane and its good compatibility with the PCL-based solid polymer electrolyte, resulting in facile ion transport and stable charge transfer reactions during cycling in the cell.

The cycling performance of the solid-state Li/$LiNi_{0.6}Co_{0.2}Mn_{0.2}O_2$ cells with different membrane-supported solid polymer electrolytes was evaluated at different current rates and 55 °C. Fig. 8a shows the discharge capacities of the cells assembled with different electrolytes as a function of the C rate. In this experiment, the current rate was increased from 0.1 to 1.0C every 5 cycles. The discharge capacities decreased with increasing C rate due to the polarization. Among the cells investigated, the cell with PEI membrane-supported solid polymer electrolyte exhibited the highest discharge capacities at high current rates, which can be attributed to lower overpotential in the cell, as previously discussed. The cell assembled with solid polymer electrolyte employing the PEI membrane exhibited a discharge capacity of 105.2 mA h g^{-1} at 1.0C rate, and a reversible capacity of 157.0 mA h g^{-1} was

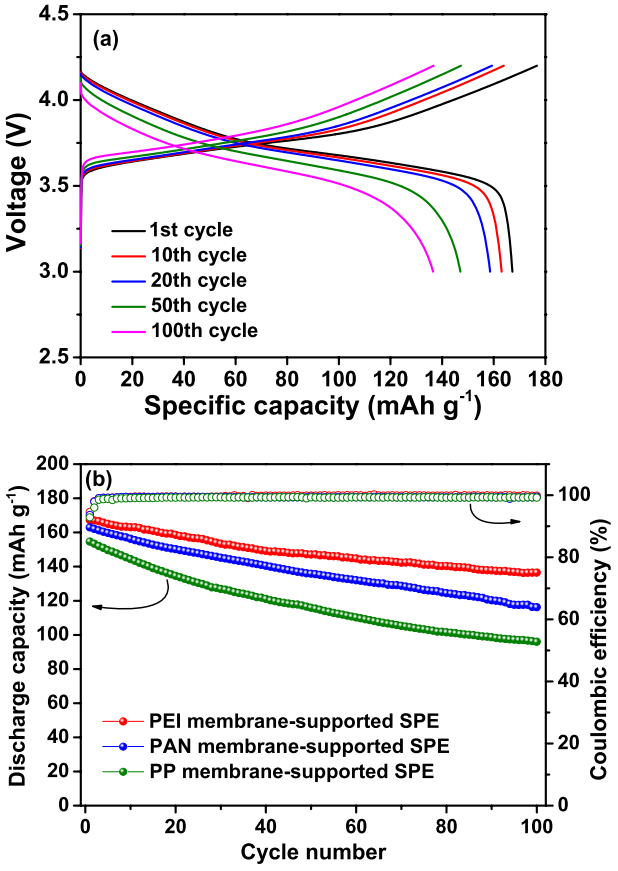

Fig. 7. (a) Charge and discharge curves of the solid-state Li/$LiNi_{0.6}Co_{0.2}Mn_{0.2}O_2$ cell assembled with PEI membrane-supported solid polymer electrolyte, and (b) discharge capacities and coulombic efficiencies of Li/$LiNi_{0.6}Co_{0.2}Mn_{0.2}O_2$ cells. Charge and discharge cycling was performed at a constant current rate of 0.1C and 55 °C.

recovered at a 0.1C rate after repeated cycling at high C rates. The cell assembled with the PEI membrane-supported solid polymer electrolyte was cycled at 0.5C rate, and the results are presented in Fig. 8b. As shown in the figure, the cell exhibited an initial discharge capacity of 148.7 mA h g^{-1} with good capacity retention. These results suggest that the PCL-based amorphous solid polymer electrolyte supported with highly porous PEI membrane can be applied as the solid electrolyte for the all-solid-state lithium cell with high capacity and good cycling stability.

4. Conclusion

Solid polymer electrolytes based on PCL and LiTFSI were prepared, and their electrochemical properties were investigated. Solid polymer electrolyte exhibited fully amorphous characteristics and low glass transition temperature at high salt concentration, resulting in high ionic conductivity. To prepare the mechanically robust free-standing film, the solid polymer electrolyte was penetrated into the pores of highly porous polymer membranes prepared from PEI, PAN and PP. The membrane-supported solid polymer electrolytes showed high electrochemical stability and good mechanical properties, which enabled their use as a solid electrolyte for all-solid-state Li cells. When the PEI was employed as the supporting membrane, the solid-state Li/$LiNi_{0.6}Co_{0.2}Mn_{0.2}O_2$ cell exhibited the best cycling performance in terms of cycling stability and rate capability, demonstrating feasible application of a PEI membrane-supported solid polymer electrolyte in the all-solid-state lithium batteries.

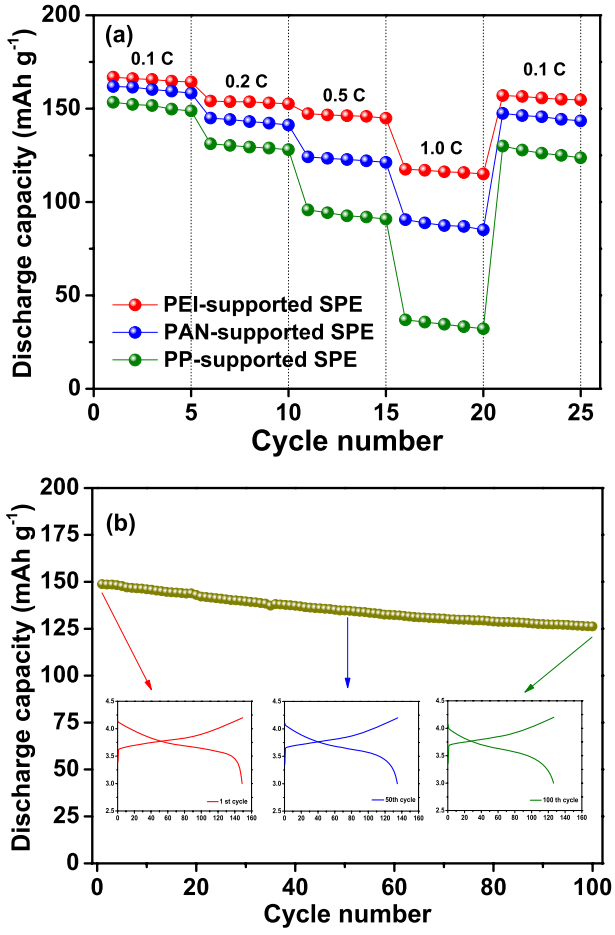

Fig. 8. (a) Discharge capacities of the solid-state Li/$LiNi_{0.6}Co_{0.2}Mn_{0.2}O_2$ cells assembled with different types of solid polymer electrolyte as a function of the C rate at 55 °C and (b) discharge capacities of the Li/$LiNi_{0.6}Co_{0.2}Mn_{0.2}O_2$ cell assembled PEI membrane-supported solid polymer electrolytes at 0.5C and 55 °C.

Declaration of competing interest

The authors declare that they have no known competing financial interests or personal relationships that could have appeared to influence the work reported in this paper.

Acknowledgements

This work was supported by the Basic Science Research Program of the National Research Foundation of Korea (NRF), funded by the Ministry of Science, ICT, and Future Planning (2017R1A2A2A05020947) and the R&D Convergence Program of the NST (National Research Council of Science & Technology) of Korea.

References

[1] M. Armand, J.M. Tarascon, Building better batteries, Nature 451 (2008) 652–657.
[2] V. Etacheri, R. Marom, R. Elazari, G. Salitra, D. Aurbach, Challenges in the development of advanced Li-ion batteries: a review, Energy Environ. Sci. 4 (2011) 3243–3262.
[3] B. Dunn, H. Kamath, J.M. Tarascon, Electrical energy storage for the grid: a battery of choices, Science 334 (2011) 928–935.
[4] J.B. Goodenough, K.S. Park, The Li-ion rechargeable battery: a perspective, J. Am. Chem. Soc. 135 (2013) 1167–1176.
[5] D. Larcher, J.M. Tarascon, Towards greener and more sustainable batteries for electrical energy storage, Nat. Chem. 7 (2015) 19–29.
[6] J.M. Tarascon, M. Armand, Issues and challenges facing rechargeable lithium batteries, Nature 414 (2001) 359.

[7] J.W. Fergus, Ceramic and polymeric solid electrolytes for lithium-ion batteries, J. Power Sources 195 (2010) 4554–4569.
[8] K. Takada, Progress and prospective of solid-state lithium batteries, Acta Mater. 61 (2013) 759–770.
[9] V. Thangadurai, S. Narayanan, D. Pinzaru, Garnet-type solid-state fast Li ion conductors for Li batteries: critical review, Chem. Soc. Rev. 43 (2014) 4714–4727.
[10] Y. Wang, W.D. Richards, S.P. Ong, L.J. Miara, J.C. Kim, Y. Mo, G. Ceder, Design principles for solid-state lithium superionic conductors, Nat. Mater. 14 (2015) 1026–1031.
[11] J. Janek, W.G. Zeier, A solid future for battery development, Nat. Energy 1 (2016) 16141.
[12] Y. Kato, S. Hori, T. Saito, K. Suzuki, M. Hirayama, A. Mitsui, M. Yonemura, H. Iba, R. Kanno, High-power all-solid-state batteries using sulfide superionic conductors, Nat. Energy 1 (2016) 16030.
[13] R. Chen, W. Qu, X. Guo, L. Li, F. Wu, The pursuit of solid-state electrolytes for lithium batteries: from comprehensive insight to emerging horizons, Mater. Horiz. 3 (2016) 487–516.
[14] S. Chen, C. Niu, H. Lee, Q. Li, L. Yu, W. Xu, J.-G. Zhang, E.J. Dufek, M. S. Whittingham, S. Meng, J. Xiao, J. Liu, Critical parameters for evaluating coin cells and pouch cells of rechargeable Li-metal batteries, Joule 3 (2019) 1094–1105.
[15] C. Niu, H. Lee, S. Chen, Q. Li, J. Du, W. Xu, J.-G. Zhang, M.S. Whittingham, J. Xiao, J. Liu, High-energy lithium metal pouch cells with limited anode swelling and long stable cycles, Nat. Energy 4 (2019) 551–559.
[16] D. Fenton, J. Parker, P. Wright, Complexes of alkali metal ions with poly(ethylene oxide), Polymer 14 (1973) 589.
[17] M. Nakayama, S. Wada, S. Kuroki, M. Nogami, Factors affecting cyclic durability of all-solid-state lithium polymer batteries using poly(ethylene oxide)-based solid polymer electrolytes, Energy Environ. Sci. 3 (2010) 1995–2002.
[18] H. Zhang, C. Liu, L. Zheng, F. Xu, W. Feng, H. Li, X. Huang, M. Armand, J. Nie, Z. Zhou, Lithium bis(fluorosulfonyl)imide/poly(ethylene oxide) polymer electrolyte, Electrochim. Acta 133 (2014) 529–538.
[19] Z. Xue, D. He, X. Xie, Poly(ethylene oxide)-based electrolytes for lithium-ion batteries, J. Mater. Chem. 3 (2015) 19218–19253.
[20] Y. Tominaga, T. Shimomura, M. Nakamura, Alternating copolymers of carbon dioxide with glycidyl ethers for novel ion-conductive polymer electrolytes, Polymer 51 (2010) 4295–4298.
[21] C.-K. Lin, I.D. Wu, Investigating the effect of interaction behavior on the ionic conductivity of Polyester/$LiClO_4$ blend systems, Polymer 52 (2011) 4106–4113.
[22] Y. Tominaga, K. Yamazaki, Fast Li-ion conduction in poly (ethylene carbonate)-based electrolytes and composites filled with TiO_2 nanoparticles, Chem. Commun. 50 (2014) 4448–4450.
[23] B. Sun, J. Mindemark, K. Edstrom, D. Brandell, Realization of high performance polycarbonate-based Li polymer batteries, Electrochem. Commun. 52 (2015) 71–74.
[24] J. Mindemark, E. Torma, B. Sun, D. Brandell, Copolymers of trimethylene carbonate and ε-caprolactone as electrolytes for lithium-ion batteries, Polymer 63 (2015) 91–98.
[25] K. Deng, S. Wang, S. Ren, D. Han, M. Xiao, Y. Meng, A novel single-ion-conducting polymer electrolyte derived from CO_2-based multifunctional polycarbonate, ACS Appl. Mater. Interfaces 8 (2016) 33642–33648.
[26] X. Liu, G. Ding, X. Zhou, S. Li, W. He, J. Chai, C. Pang, Z. Liu, G. Cui, An interpenetrating network poly(diethylene glycol carbonate)-based polymer electrolyte for solid state lithium batteries, J. Mater. Chem. 5 (2017) 11124–11130.
[27] T. Morioka, K. Nakano, Y. Tominaga, Ion-conductive properties of a polymer electrolyte based on ethylene carbonate/ethylene oxide random copolymer, Macromol. Rapid Commun. (2017) 1600652.
[28] Y.-C. Jung, M.-S. Park, D.-H. Kim, M. Ue, A. Eftekhari, D.-W. Kim, Room-temperature performance of poly(ethylene ether carbonate)-based solid polymer electrolytes for all-solid-state lithium batteries, Sci. Rep. 7 (2017) 17482.
[29] M.-S. Park, Y.-C. Jung, D.-W. Kim, Hybrid solid electrolytes composed of poly(1,4-butylene adipate) and lithium aluminum germanium phosphate for all-solid-state $Li/LiNi_{0.6}Co_{0.2}Mn_{0.2}O_2$ cells, Solid State Ionics 315 (2018) 65–70.
[30] M. Watanabe, M. Rikukawa, K. Sanui, N. Ogata, H. Kato, T. Kobayashi, Z. Ohtaki, Ionic conductivity of polymer complexes formed by poly(ethylene succinate) and lithium perchlorate, Macromolecules 17 (1984) 2902–2908.
[31] R.D. Armstrong, M.D. Clarke, Lithium ion conducting polymeric electrolytes based on poly(ethylene adipate), Electrochim. Acta 29 (1984) 1443–1446.
[32] R. Dupon, B.L. Papke, M.A. Ratner, D.F. Shriver, Ion-transport in the polymer electrolytes formed between poly(ethylene succinate) and lithium tetrafluoroborate, J. Electrochem. Soc. 131 (1984) 586–589.
[33] M. Watanabe, M. Rikukawa, K. Sanui, N. Ogata, Effects of polymer structure and incorporated salt species on ionic-conductivity of polymer complexes formed by aliphatic polyester and alkali-metal thiocyanate, Macromolecules 19 (1986) 188–192.
[34] D.-W. Kim, J.-S. Song, J.-K. Park, Synthesis, characterization and electrical properties of the novel polymer electrolytes based on polyesters containing ethylene oxide moiety, Electrochim. Acta 40 (1995) 1697–1700.
[35] Y.C. Lee, M.A. Ratner, D.F. Shriver, Ionic conductivity in the poly(ethylene malonate)/lithium triflate system, Solid State Ionics 138 (2001) 273–276.
[36] C.K. Lin, I.D. Wu, Investigating the effect of interaction behavior on the ionic conductivity of polyester/$LiClO_4$ blend systems, Polymer 52 (2011) 4106–4113.
[37] J. Mindemark, B. Sun, E. Torma, D. Brandell, High-performance solid polymer electrolytes for lithium batteries operational at ambient temperature, J. Power Sources 298 (2015) 166–170.
[38] C.-G. Wu, M.-I. Lu, H.-J. Chuang, PVdF-HFP/P123 hybrid with mesopores: a new matrix for high-conducting, low-leakage porous polymer electrolyte, Polymer 46 (2005) 5929–5938.
[39] T. Ma, Z. Cui, Y. Wu, S. Qin, H. Wang, F. Yan, N. Han, J. Li, Preparation of PVDF based blend microporous membranes for lithium ion batteries by thermally induced phase separation: I. Effect of PMMA on the membrane formation process and the properties, J. Membr. Sci. 444 (2013) 213–222.
[40] D.-W. Kim, J.-K. Park, M.-S. Gong, Conductivity studies of polymer electrolytes based on apliphatic polyesters, J. Polym. Sci., Polym. Phys. Ed. 33 (1995) 1323–1331.
[41] E. Quartarone, P. Mustarelli, Electrolytes for solid-state lithium rechargeable batteries: recent advances and perspectives, Chem. Soc. Rev. 40 (2011) 2525–2540.
[42] N. Gokalp, C. Ulker, Y.A. Guvenilir, Synthesis of polycaprolactone via ring opening polymerization catalyzed by Candida Antarctica lipase B immobilized onto an amorphous silica support, J. Polym. Mater. 33 (2016) 87–100.